Article

Oxyanion Selectivity in Sulfate and Molybdate Transport Proteins: An ab Initio/CDM Study

Todor Dudev, and Carmay Lim

J. Am. Chem. Soc., **2004**, 126 (33), 10296-10305• DOI: 10.1021/ja047951n • Publication Date (Web): 03 August 2004

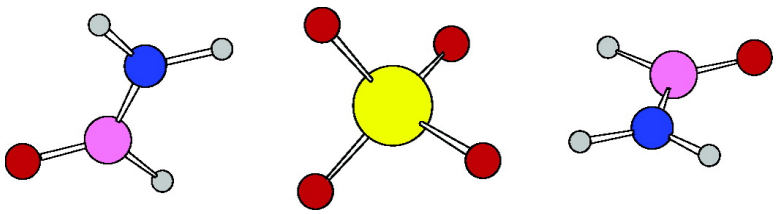

J|A|C|S
ARTICLES
Published on Web 08/03/2004

Oxyanion Selectivity in Sulfate and Molybdate Transport Proteins: An ab Initio/CDM Study

Todor Dudev† and Carmay Lim*,†,‡

Contribution from the Institute of Biomedical Sciences, Academia Sinica, Taipei 11529, Taiwan, R.O.C., and Department of Chemistry, National Tsing Hua University, Hsinchu 300, Taiwan, R.O.C.

Received April 8, 2004; E-mail: carmay@gate.sinica.edu.tw

Abstract: A striking feature of sulfate (SO_4^{2-}) and molybdate (MoO_4^{2-}) transport proteins, such as SBP and ModA, which specifically bind SO_4^{2-} and MoO_4^{2-}, respectively, is their ability to discriminate very similar anions with the same net charge, geometry, and hydrogen-bonding properties. Here, we determine to what extent (1) oxyanion−solvent interactions, (2) oxyanion−amino acid interactions, and (3) the anion-binding pocket sizes of the cognate protein contribute to the anion selectivity process in SO_4^{2-} and MoO_4^{2-} transport proteins by computing the free energies for replacing SO_4^{2-} with MoO_4^{2-}/WO_4^{2-} in model SO_4^{2-}-binding sites of varying degrees of solvent exposure using a combined quantum mechanical/continuum dielectric approach. The calculations reveal that MoO_4^{2-} transport proteins, such as ModA, specifically bind MoO_4^{2-}/WO_4^{2-} but not SO_4^{2-}, mainly because the desolvation penalty of MoO_4^{2-}/WO_4^{2-} is significantly less than that of SO_4^{2-} and, to a lesser extent, because the large and rigid cavity in these proteins attenuates ligand interactions with SO_4^{2-}, as compared to MoO_4^{2-}. On the other hand, SO_4^{2-} transport proteins prefer SO_4^{2-} to MoO_4^{2-}/WO_4^{2-} because the small anion-binding pocket characteristic of these proteins inhibits binding of the larger MoO_4^{2-} and WO_4^{2-} anions. The calculations also help to explain the absence of positively charged Lys/Arg side chains in the anion-binding sites of SBP and ModA. During evolution, these transport proteins may have excluded cationic ligands from their binding sites because, on one hand, Lys/Arg do not contribute to the selectivity of the binding pocket and, on the other, they substantially stabilize the complex between the oxyanion and protein ligands, which in turn would prohibit the rapid release of the bound oxyanion at a certain stage during the transport process.

Introduction

Elucidating the factors governing cation/anion selectivity in proteins is of major importance in studying their evolution, structure, and function. In selecting the natural ionic cofactor-(s) from the surrounding fluids, different proteins have adopted different strategies. In most cases the *cationic*-binding site's ligand composition dictates the cation selectivity. Thus, binding sites containing "soft" ligands such as cysteine and histidine are highly specific for the "borderline" zinc dication and are well protected against "hard" dications such as Mg^{2+} and Ca^{2+}, which are much more abundant in the cellular fluids.[1−3] The metal-binding cavity size is another factor that contributes to the cation selectivity. For example, the fine-tuning of the metal-binding cavity size allows EF-hand-like proteins to bind Ca^{2+} more favorably than its natural competitor Mg^{2+}.[4,5] In some cases such as azurin[6] and carbonic anhydrase,[7,8] the metal-binding site's geometry selects for a given cation by negative design; i.e., the specific arrangement and directionality of the first-shell ligands, which are optimized to best fit the natural cofactor's coordination requirements, disfavor binding of competing cations with different coordination geometries. The metal-binding site's total charge may also play a role in discriminating between cations with different charges. For example, some Ca-binding sites with a total ligand charge of −3 can sequester the natural cofactor Ca^{2+} from cellular solutions containing much higher concentrations of monovalent ions such as Na^+ and K^+.[4,5] However, some cation-binding sites such as Mg^{2+}-sites appear not to be very specific for their natural cofactors suggesting that these cofactors have been chosen based mainly on their natural abundance in living cells. In such cases, it seems that it is not the *protein* itself that has evolved to select the particular cofactor from other cations. Instead, it is the *cell machinery* that orchestrates the process of cation binding by regulating appropriate concentrations of the natural cofactor and other competing cations in various biological compartments.[3,9]

† Academia Sinica.
‡ National Tsing Hua University.

(1) Lee, L. V.; Poyner, R. R.; Vu, M. V.; Cleland, W. W. *Biochemistry* **2000**, *39*, 4821−4830.
(2) Huang, D. T. C.; Thomas, M. A. W.; Christopherson, R. I. *Biochemistry* **1999**, *38*, 9964−9970.
(3) Dudev, T.; Lim, C. *J. Phys. Chem. B* **2001**, *105*, 4446−4452.
(4) Falke, J. J.; Snyder, E. E.; Thatcher, K. C.; Voertler, C. S. *Biochemistry* **1991**, *30*, 8690−8697.
(5) Drake, S. K.; Zimmer, M. A.; Kundrot, C.; Falke, J. J. *J. Gen. Physiol.* **1997**, *110*, 173−184.
(6) Engeseth, H. R.; McMillin, D. R. *Biochemistry* **1986**, *25*, 2448−2455.
(7) Cox, E. H.; Hunt, J. A.; Compher, K. M.; Fierke, C. A.; Christianson, D. W. *Biochemistry* **2000**, *39*, 13687−13694.
(8) Hunt, J. A.; Ahmed, M.; Fierke, C. A. *Biochemistry* **1999**, *38*, 9054−9062.
(9) Dudev, T.; Lim, C. *Chem. Rev.* **2003**, *103*, 773−787.

10.1021/ja047951n CCC: $27.50

Several of the factors that contribute to *cation* selectivity such as the protein ligand composition and cavity size have also been reported to contribute to *anion* selectivity by proteins. The *anion-binding site's ligand composition* has been shown to dictate the anion selectivity of phosphate vs sulfate transport proteins. Compared to the transport sulfate-binding protein (SBP), the phosphate transport protein contains in its anionic-binding site one or two more Asp residues,[10−12] whose carboxylate side chain(s) can hydrogen bond to the proton(s) of the HPO_4^{2-} or $H_2PO_4^-$ cofactor but would repel fully ionized anions such as SO_4^{2-}. This enables the phosphate transport protein to bind selectively and tightly to its natural cofactor and to reject sulfate dianions, which at normal pH exist as SO_4^{2-}.[10] On the other hand, the SBP contains in its anionic-binding site only neutral hydrogen-bond-donating ligands and no acidic side chain residue(s), in contrast to the phosphate transport protein's binding site.[13,14] This enables the SBP to discriminate between SO_4^{2-} (the natural cofactor) and phosphate anions: SBP binds SO_4^{2-} with a binding constant K_a of 8.33×10^6 M^{-1}, while it binds HPO_4^{2-} and $H_2PO_4^-$ with a K_a of ∼17 and ∼1 M^{-1}, respectively.[14]

The *anion size* has been postulated to dictate the anion selectivity of sulfate vs molybdate transport proteins.[15,16] For example, the SBP binds SO_4^{2-} with high affinity ($K_a = 8.33 \times 10^6$ M^{-1})[14] but MoO_4^{2-} with very low affinity,[17] whereas the molybdate transport protein, ModA, binds MoO_4^{2-} ($K_a = 5.0 \times 10^7$ M^{-1})[15] but not sulfate or phosphate. However, the binding sites of SBP and ModA are strikingly similar in that they are rigid, deeply buried, and lined by seven hydrogen-bond-accepting entities such as main chain and side chain NH and side chain OH groups.[13,16,18] Therefore, the ligand size has been postulated to be the major determinant of selectivity in ModA and SBP.[15,16] This is based on the following experimental observations. First, ModA also binds tungstate (WO_4^{2-}) with almost the same affinity as MoO_4^{2-}.[15,19] Second, the metal−O distances for WO_4^{2-} (W−O = 1.78−1.79 Å) and MoO_4^{2-} (Mo−O = 1.75−1.78 Å) are similar and significantly longer than for SO_4^{2-} (S−O = 1.47−1.49 Å).[20] Third, although the anion-binding pockets of molybdate-binding proteins from *A. vinelandii* (ModA2) and *E. coli* (EcModA) are lined by different amino acid residues, they are similar in size and significantly bigger than the SBP pocket.[16]

Differences in the oxyanion size would not only translate into differences in the anion-binding pockets of the cognate protein but also would be expected to result in differences in oxyanion−amino acid interactions on one hand and differences in oxyanion−solvent interactions on the other. For example, replacing MoO_4^{2-} with the much smaller SO_4^{2-} in the *rigid* (see above) anion-binding site of ModA would likely attenuate the hydrogen-bonding interactions between the oxyanion and the protein ligands. Furthermore, upon receptor binding, the desolvation penalty of SO_4^{2-} could be more costly than that of MoO_4^{2-}/WO_4^{2-}, as the hydration free energy of SO_4^{2-} is expected to be more favorable than that of the much larger MoO_4^{2-}/WO_4^{2-}. Thus, in this work we examine whether and to what extent differences in (1) the desolvation penalties of the oxyanions upon receptor binding, (2) the oxyanion−ligand interactions, and (3) the cavity sizes contribute to the anion selectivity process in sulfate and molybdate transport proteins. Furthermore, we attempt to elucidate why the anionic-binding sites in SBP and ModA contain only noncharged amino acid ligands and lack positively charged residues, which, in other (nontransport) sulfate and molybdate-binding proteins, are found to electrostatically stabilize the bound anion.[21,22] To address the above questions, we employ quantum mechanical calculations in conjunction with continuum dielectric methods. To the best of our knowledge, no theoretical calculations have been performed to elucidate the mechanism of oxyanion binding in these systems. First the calculations are calibrated against available experimental data. Next, the free energies are evaluated in both the gas phase and condensed media for $SO_4^{2-} \rightarrow MoO_4^{2-}$/$WO_4^{2-}$ exchange reactions in model sulfate-binding sites. The theoretical findings are compared with experimental data, and the factors governing the anion selectivity in SBP and ModA proteins are discussed in the last section.

Methods

Models Used. The X-ray structures of SBP[13] and ModA[16,23] show the oxyanion heptacoordinated to Asn, Trp, Ser, Thr, and Tyr side chains as well as the backbone amide. The backbone peptide group and Asn/Gln side chains were modeled by formamide ($HCONH_2$), while Ser/Thr and Lys side chains were modeled by methanol (CH_3OH) and methylammonium cation ($CH_3NH_3^+$), respectively.

For a given model $[(SO_4)\cdot L_n]^{2-}$ binding site, where L = $HCONH_2$ or CH_3OH, and $n = 1-7$, the energies/free energies for replacing SO_4^{2-} with MoO_4^{2-}/WO_4^{2-} were computed in various dielectric media; i.e.,

$$[(SO_4)\cdot L_n]^{2-} + XO_4^{2-} \leftrightarrow [(XO_4)\cdot L_n]^{2-} + SO_4^{2-} \qquad (1)$$

where X = Mo or W. As SO_4^{2-}, MoO_4^{2-}, and WO_4^{2-} are found to be completely dehydrated in the respective protein binding sites,[13,16,18] complexes with explicit water(s) bound to the oxyanion were not considered. For mono-, bi-, tri-, and tetracoordinated complexes, trends in the *free energies* for eq 1 were analyzed. However, the high basis set used in the present calculations prevented us from evaluating vibrational frequencies (and thus thermal and entropic corrections to the electronic energy; see below) of complexes with more than four ligands coordinated to the oxyanion. Thus, for penta-, hexa-, and heptacoordinated complexes, trends in the reaction *energies* ΔE were analyzed (see Results section).

Determining the Optimal Theory/Basis Set Level for Geometry Optimization. The series of tetrahedral dianions, SO_4^{2-}, SeO_4^{2-}, CrO_4^{2-}, MoO_4^{2-}, and WO_4^{2-}, were used to calibrate the predicted geometries. The geometries of these dianions were fully optimized using Møller−Plesset second-order perturbation theory (MP2),[24,25] as well

(10) Luecke, H.; Quiocho, F. A. *Nature* **1990**, *347*, 402−406.
(11) Vyas, N. K.; Vyas, M. N.; Quiocho, F. A. *Structure* **2003**, *11*, 765−774.
(12) Ledvina, P. S.; Yao, N.; Choudhary, A.; Quiocho, F. A. *Proc. Natl. Acad. Sci. U.S.A.* **1996**, *93*, 6786−6791.
(13) Pflugrath, J. W.; Quiocho, F. A. *Nature* **1985**, *314*, 257−260.
(14) Jacobson, B. L.; Quiocho, F. A. *J. Mol. Biol.* **1988**, *204*, 783−787.
(15) Imperial, J.; Hadi, M.; Amy, N. K. *Biochim. Biophys. Acta* **1998**, *1370*, 337−346.
(16) Lawson, D. M.; Williams, C. E. M.; Mitchenall, L. A.; Pau, R. N. *Structure* **1998**, *6*, 1529−1539.
(17) Pardee, A. B.; Prestidge, L. S.; Whipple, M. B.; Dreyfuss, J. *J. Biol. Chem.* **1966**, *241*, 3962−3969.
(18) Lawson, D. M.; Williams, C. E. M.; White, D. J.; Choay, A. P.; Mitchenall, L. A.; Pau, R. N. *J. Chem. Soc., Dalton Trans.* **1997**, 3981−3984.
(19) Rech, S.; Wolin, C.; Gunsalus, R. P. *J. Biol. Chem.* **1996**, *271*, 2557−2562.
(20) Bridgeman, A. J.; Cavigliasso, G. *Polyhedron* **2001**, *20*, 2269−2277.
(21) Chakrabarti, P. *J. Mol. Biol.* **1993**, *234*, 463−482.
(22) Gourley, D. G.; Schuttelkopf, A. W.; Anderson, L. A.; Price, N. C.; Boxer, D. H.; Hunter, W. N. *J. Biol. Chem.* **2001**, *276*, 20641−20647.
(23) Hu, Y.; Rech, S.; Gunsalus, R. P.; Rees, D. C. *Nat. Struct. Biol.* **1997**, *4*, 703−707.
(24) Frisch, M. J.; Head-Gordon, M.; Pople, J. A. *Chem. Phys. Lett.* **1990**, *166*, 281−289.

Table 1. Calculated and Experimental X−O Bond Lengths (in Å) for XO_4^{2-} Anions (X = S, Se, Cr, Mo, and W)

	MP2	B3-LYP	S-VWN	experiment
		SO_4^{2-}		
6-31+G(d)	1.531	1.532	1.527	1.47−1.49[a]
6-311++G(d,p)	1.518	1.527	1.521	1.47 ± 0.02[b]
6-311++G(2d,2p)	1.510	1.513	1.506	
6-311++G(2df,2p)	1.503	1.509	1.502	
6-311++G(3df,3pd)	1.496	1.501	1.495	
		SeO_4^{2-}		
6-31+G(d)	1.681	1.689	1.680	1.64−1.65[a]
6-311++G(d,p)	1.674	1.691	1.680	1.63 ± 0.02[c]
6-311++G(2d,2p)	1.667	1.679	1.669	
6-311++G(2df,2p)	1.656	1.669	1.660	
6-311++G(3df,3pd)	1.657	1.669	1.660	
		CrO_4^{2-}		
6-31+G(d)	1.699	1.657	1.648	1.65[a]
6-311++G(d,p)	1.692	1.658	1.650	1.63 ± 0.03[c]
6-311++G(2d,2p)	1.698	1.660	1.652	
6-311++G(2df,2p)	1.693	1.658	1.650	
6-311++G(3df,3pd)	1.692	1.657	1.649	
		MoO_4^{2-}		
6-31+G(d)	1.832	1.800	1.792	1.75−1.78[a]
6-311++G(d,p)	1.837	1.805	1.797	1.75 ± 0.04[b]
6-311++G(2d,2p)	1.824	1.799	1.791	
6-311++G(2df,2p)	1.813	1.796	1.788	
6-311++G(3df,3pd)	1.820	1.798	1.790	
		WO_4^{2-}		
6-31+G(d)	1.835	1.815	1.807	1.78−1.79[a]
6-311++G(d,p)	1.839	1.819	1.812	1.76 ± 0.02[c]
6-311++G(2d,2p)	1.828	1.814	1.806	
6-311++G(2df,2p)	1.818	1.814	1.803	
6-311++G(3df,3pd)	1.825	1.813	1.805	

[a] Taken from ref 20. [b] Average bond lengths from analysis of Cambridge Structure Database (CSD) structures taken from ref 16. [c] Average bond lengths from analysis of CSD structures; this work.

as density functional theory (DFT) with the B3-LYP[26,27] and S-VWN[28,29] functionals in conjunction with different basis sets. Stuttgart−Dresden SDD basis set/ECP was used for molybdenum and tungsten,[30] while the full-electron basis sets listed in Table 1 were used for the other atom types (O, S, Se, and Cr). T_d spherical symmetry was assumed for each of the species. Comparison of the computed and experimental bond distances in Table 1 shows that, among the various methods, S-VWN/6-311++G(2df,2p) best reproduced the test set of tetrahedral dianion geometries (see Results section). Consequently, *full* geometry optimization of each anion complex in eq 1 was carried out at the S-VWN/6-311++G(2df,2p) level using the Gaussian 03 program.[30] Vibrational frequencies were then computed at the same level of theory/basis set to verify that each complex was at the minimum of its potential energy surface. *No* imaginary frequency was found in any of the complexes.

Table 2. Gas-Phase Free Energies (in kcal/mol) for $H_2SO_4 + H^+ \rightarrow H_3SO_4^+$ Calculated at Different Levels of Theory[a]

	MP2	B3-LYP	S-VWN
6-31+G(d)	−155.5	−159.4	−155.9
6-311++G(d,p)	−163.4	−162.6	−158.3
6-311++G(2d,2p)	−162.8	−164.4	−159.9
6-311++G(2df,2p)	−162.6	−164.8	−160.4
6-311++G(3df,3pd)	−163.9	−165.1	−160.8

[a] The geometries, thermal energies, and entropies of H_2SO_4 and $H_3SO_4^+$ were evaluated at the S-VWN/6-311++G(2df,2p) level, while the electronic energy was corrected using single-point calculations with different methods.

Scheme 1

$$\begin{array}{ccc} & \Delta G^1 & \\ \text{Reactants } (\varepsilon = 1) & \rightarrow & \text{Products } (\varepsilon = 1) \\ \Delta G_{solv}{}^x \text{ (Reactants)} \downarrow & & \downarrow \Delta G_{solv}{}^x \text{ (Products)} \\ \text{Reactants } (\varepsilon = x) & \rightarrow & \text{Products } (\varepsilon = x) \\ & \Delta G^x & \end{array}$$

Computing the Gas-Phase Free Energy. Based on the fully optimized geometries of the free and complexed oxyanions, the gas-phase free energies for eq 1 at a temperature $T = 298.15$ K were computed according to

$$\Delta G^1 = \Delta E_{elec} + \Delta E_T + \Delta PV - T\Delta S \qquad (2)$$

where ΔE_{elec}, ΔE_T, ΔPV, and ΔS are the differences in the electronic energy, thermal energy (including the zero-point energy), work term, and entropy between the product(s) and reactant(s), respectively. In computation of the thermal energy and vibrational entropy, the S-VWN/6-311++G(2df,2p) frequencies were scaled by an empirical factor of 0.9833.[31]

Determining the Optimal Theory/Basis Set Level for Gas-Phase Free Energy Calculations. The experimental gas-phase protonation free energy for

$$H_2SO_4 + H^+ \rightarrow H_3SO_4^+ \qquad (3)$$

was used to calibrate the computed gas-phase free energies. The geometries, thermal energy, and vibrational entropy of H_2SO_4 and $H_3SO_4^+$ were evaluated at the S-VWN/6-311++G(2df,2p) level, while the electronic energies were computed using the same combinations of methods and basis sets used to calibrate the geometries. Comparison of the gas-phase proton free energies computed using eq 2 with the corresponding experimental free energy for eq 3 in Table 2 showed that the electronic energies corrected at the MP2/6-311++G(d,p) level yielded a free energy that best matched the experimental number (see Results section). Accordingly, single-point calculations at MP2/6-311++G(d,p) were used to compute the electronic energies.

Exchange Free Energies. The reaction free energy in a given environment characterized by a dielectric constant $\epsilon = x$ can be calculated using the following thermodynamic cycle (Scheme 1).

ΔG^1 is the gas-phase free energy computed using eq 2, while $\Delta G_{solv}{}^x$ is the free energy for transferring a molecule in the gas phase to a continuous solvent medium characterized by a dielectric constant, x. By solving Poisson's equation using finite difference methods[32,33] to

(25) Head-Gordon, M.; Head-Gordon, T. *Chem. Phys. Lett.* **1994**, *220*, 122−128.
(26) Becke, A. D. *J. Chem. Phys* **1993**, *98*, 5648−5652.
(27) Lee, C.; Yang, W.; Parr, R. G. *Phys. Rev.* **1988**, *B37*, 785−789.
(28) Slater, J. C. *Quantum theory of molecules and solids. Vol. 4: The self-consistent field for molecules and solids*; McGraw-Hill: New York, 1974.
(29) Vosko, S. H.; Wilk, L.; Nusair, M. *Can. J. Phys.* **1980**, *58*, 1200−1211.
(30) Frisch, M. J.; Trucks, G. W.; Schlegel, H. B.; Scuseria, G. E.; Robb, M. A.; Cheeseman, J. R.; Montgomery, J. A., Jr.; Vreven, T.; Kudin, K. N.; Burant, J. C.; Millam, J. M.; Iyengar, S. S.; Tomasi, J.; Barone, V.; Mennucci, B.; Cossi, M.; Scalmani, G.; Rega, N.; Peterson, G. A.; Nakatsuji, H.; Hada, M.; Ehara, M.; Toyota, K.; Fukuda, R.; Hasegawa, J.; Ishida, M.; Nakajima, T.; Honda, Y.; Kitao, O.; Nakai, H.; Klene, M.; Li, X.; Knox, J. E.; Hratchian, H. P.; Cross, J. B.; Adamo, C.; Jaramillo, J.; Gomperts, R.; Stratmann, R. E.; Yazyev, O.; Austin, A. J.; Cammi, R.; Pomelli, C.; Ochterski, J. W.; Ayala, P. Y.; Morokuma, K.; Voth, G. A.; Salvador, P.; Dannenberg, J. J.; Zakrzewski, V. G.; Dapprich, S.; Daniels, A. D.; Strain, M. C.; Farkas, O.; Malick, D. K.; Rabuck, A. D.; Raghavachari, K.; Foresman, J. B.; Ortiz, J. V.; Cui, Q.; Baboul, A. G.; Clifford, S.; Cioslovski, J.; Stefanov, B. B.; Liu, G.; Liasehenko, A.; Piskorz, P.; Komaromi, I.; Martin, R. L.; Fox, D. J.; Keith, T.; Al-Laham, M. A.; Peng, C. Y.; Nanayakkara, A.; Challacombe, M.; Gill, P. M. W.; Johnson, B.; Chen, W.; Wong, M. W.; Gonzalez, C.; Pople, J. A. *Gaussian 03*, rev. B.03; Gaussian, Inc.: Pittsburgh, PA, 2003.
(31) Wong, M. W. *Chem. Phys. Lett.* **1996**, *256*, 391−399.
(32) Gilson, M. K.; Honig, B. *Biopolymers* **1986**, *25*, 2097−2119.
(33) Lim, C.; Bashford, D.; Karplus, M. *J. Phys. Chem.* **1991**, *95*, 5610−5620.

estimate $\Delta G_{solv}{}^{x}$ (see below), the reaction free energy in an environment modeled by dielectric constant x, ΔG^{x}, can be computed from

$$\Delta G^{x} = \Delta G^{1} + \Delta G_{solv}{}^{x}(\text{Products}) - \Delta G_{solv}{}^{x}(\text{Reactants}) \quad (4)$$

The continuum dielectric calculations employed a 71 × 71 × 71 lattice with an initial grid spacing of 1.0 Å and were refined with a spacing of 0.25 Å. The low-dielectric region of the solute was defined as the region inaccessible to contact by a 1.4 Å radius sphere rolling over the molecular surface. This region was assigned an internal dielectric constant, ϵ_{in}, of 2 to account for the electronic polarizability of the solute. The molecular surface was defined by effective solute radii, which were obtained by adjusting the CHARMM27[34] van der Waals radii to reproduce the experimental hydration free energies of the oxyanions and ligands (see Results section). These radii were optimized for S-VWN/6-311++G(2df,2p) geometries and natural bond orbital (NBO)[35] atomic charges. They are as follows (in Å): $R_S = 2.00$, $R_{Mo} = 2.75$, $R_W = 2.93$, $R_O(XO_4) = 1.64$, $R_O(C) = 1.85$, $R_N = 1.85$, $R_C = 1.95$, $R_H(N,O) = 1.38$, $R_H(C) = 1.468$. Thus, Poisson's equation was solved with an external dielectric constant ϵ_{out} equal to 1, 4, 10, 20, and 80 to mimic binding sites of varying degrees of solvent exposure. The difference between the computed electrostatic potentials in a given dielectric medium ($\epsilon_{out} = x$) and in the gas phase ($\epsilon_{out} = 1$) yielded the solvation free energy $\Delta G_{solv}{}^{x}$ of the studied molecule.

Results

Geometry Calibration. To determine the optimal theory/basis set level for geometry optimization, different methods in conjunction with various basis sets (see Methods) were used to evaluate the molecular geometries for tetrahedral SO_4^{2-}, SeO_4^{2-}, CrO_4^{2-}, MoO_4^{2-}, and WO_4^{2-} dianions. Comparison of the calculated and X-ray bond lengths in Table 1 shows that the calculations generally overestimate the measured bond length. This is partly because the computed bond lengths correspond to (isolated) gas-phase structures, while the measured bond lengths are derived from crystal structures that may be affected by the nature of the counterions and crystal packing. Table 1 shows that MP2 combined with the larger basis sets, 6-311++G(2df,2p) and 6-311++G(3df,3pd), performs well for SO_4^{2-} and SeO_4^{2-}, but produces unsatisfactory results for the other dianions: the deviations from the experimental bond distances are 0.04−0.06 Å, 0.03−0.07 Å, and 0.03−0.06 Å for CrO_4^{2-}, MoO_4^{2-}, and WO_4^{2-}, respectively. Compared to MP2, the two DFT methods yield M−O (M = Cr, Mo, W) distances that are in better agreement with experiment. Relative to B3-LYP, S-VWN yields shorter bond lengths (by ~0.01 Å) that are closer to the respective experimental values. These observations are in line with those of Bridgeman and Cavigliasso, who have also found that local density approximation calculations using the VWN functional for the entire series of tetrahedral oxyanions XO_4^{n-} (X = Si, P, S, Cl, Ge, As, Se, Br, I, Ti, V, Cr, Mn, Nb, Mo, Tc, Ta, W, and Re; $n = 1-4$) yield better geometry than calculations using B3-LYP and B-P86 functionals.[20] The S-VWN functional in conjunction with the 6-311++G(2df,2p) and 6-311++G(3df,3pd) basis sets reproduces all the experimental bond lengths in Table 1 to within 0.015 Å, which is within the experimental error bar. Among these two methods, S-VWN/6-311++G(2df,2p), being computationally more economical, was chosen for subsequent geometry calculations.

Gas-Phase Free Energy Calibration. To determine the optimal theory/basis set level for gas-phase free energy calculations, we searched the literature for experimental gas-phase energies/free energies of reactions involving XO_4^{2-} (X = S, Mo, W) but could not find such experimental values. However, we found that the gas-phase protonation free energy of H_2SO_4, the closest relative to the oxyanions of interest, has been measured.[36] Thus, different methods in conjunction with various basis sets (see Methods) were used to evaluate the gas-phase protonation free energy for $H_2SO_4 + H^+ \rightarrow H_3SO_4^+$ (eq 3). Comparison of the computed numbers in Table 2 with the corresponding experimental value of -163.2 ± 1.2 kcal/mol[36] shows that the double-ζ basis set yields unsatisfactory results while the triple-ζ basis sets significantly improve the agreement with the experiment. However, the S-VWN functional, in conjunction with the highest basis set, fails to reproduce the experimental free energy. The best results are achieved with E_{elec} corrected at the MP2 level, where all the triple-ζ basis sets reproduce the experimental free energy to within experimental error. As MP2/6-311++G(d,p) gives the best match with the experimental number and is, at the same time, computationally affordable, it was chosen for evaluating the energy corrections of the species studied.

Estimating the Hydration Free Energies of MoO_4^{2-} and WO_4^{2-}. Experimental hydration free energies, $\Delta G_{solv}{}^{80}$, are not available for MoO_4^{2-} and WO_4^{2-}. However, $\Delta G_{solv}{}^{80}$ have been measured for oxyanions such as SO_4^{2-}, CrO_4^{2-}, SeO_4^{2-}, and PO_4^{3-}, and some other spherical anions such as SiF_6^{2-}, F^-, Cl^-, Br^-, BF_4^-, and BPh_4^-.[37] These experimental values were used to estimate the hydration free energies of molybdate and tungstate by plotting them against q^2/R_{ion}, where q is the net anion charge and R_{ion} is the respective Pauling-type ionic radius of the spherical anion taken from ref 37. Figure 1 shows a good linear correlation between $\Delta G_{solv}{}^{80}$ and q^2/R_{ion} with a correlation coefficient $r^2 = 0.990$. $\Delta G_{solv}{}^{80}$ can be approximated by

$$\Delta G_{solv}{}^{80} \approx -180.07 q^2/R_{ion} + 38.46 \quad (5)$$

The hydration free energy, $\Delta G_{solv}{}^{80}$, of SO_4^{2-} (−257.3 kcal/mol) predicted using eq 5 with $q = -2$ and $R_{ion}(SO_4^{2-}) = 2.40$ Å[37] is close to the experimental value of −258.1 kcal/mol. Thus, eq 5 with $q = -2$, $R_{ion}(MoO_4^{2-}) = 2.68$ Å, and $R_{ion}(WO_4^{2-}) = 2.71$ Å[37] predicts that $\Delta G_{solv}{}^{80}(MoO_4^{2-}) = -230.3$ kcal/mol, while $\Delta G_{solv}{}^{80}(WO_4^{2-}) = -227.3$ kcal/mol. To reproduce these solvation free energies, the continuum dielectric calculations were performed using $R_{Mo} = 2.75$ Å, $R_W = 2.93$ Å, $R_O(XO_4) = 1.64$ Å (see Methods). The resulting $\Delta G_{solv}{}^{80}$ for MoO_4^{2-} (−230.1 kcal/mol) and WO_4^{2-} (−226.9 kcal/mol) are in close agreement with the respective interpolated values of −230.3 and −227.3 kcal/mol, respectively.

Solvation Free Energy Calibration. The experimental solvation free energies of sulfate and the model ligands under study were used to calibrate the solvation free energy calculations. The combination of effective atomic radii listed in the Methods section and NBO charges and geometries evaluated

(34) MacKerell, J. A. D.; Bashford, D.; Bellott, M.; Dunbrack, R.; Evanseck, J. D.; Field, M. J.; Fischer, S.; Gao, J.; Guo, H.; Ha, S.; Joseph-McCarthy, D.; Kuchnir, L.; Kuczera, K.; Lau, F. T. K.; Mattos, C.; Michnick, S.; Ngo, T.; Nguyen, D. T.; Prodhom, B.; Reiher, W. E. I.; Roux, B.; Schlenkrich, M.; Smith, J. C.; Stote, R.; Straub, J.; Watanabe, M.; Wiorkiewicz-Kuczera, J.; Yin, D.; Karplus, M. *J. Phys. Chem. B.* **1998**, *102*, 3586−3616.
(35) Reed, A. E.; Curtiss, L. A.; Weinhold, F. *Chem. Rev.* **1988**, *88*, 899−926.
(36) Do, K.; Klein, T. P.; Pommerening, C. A.; Bachrach, S. M.; Sunderlin, L. S. *J. Am. Chem. Soc* **1998**, *120*, 6093−6096.
(37) Marcus, Y. *Biophys. Chem.* **1994**, *51*, 111−127.

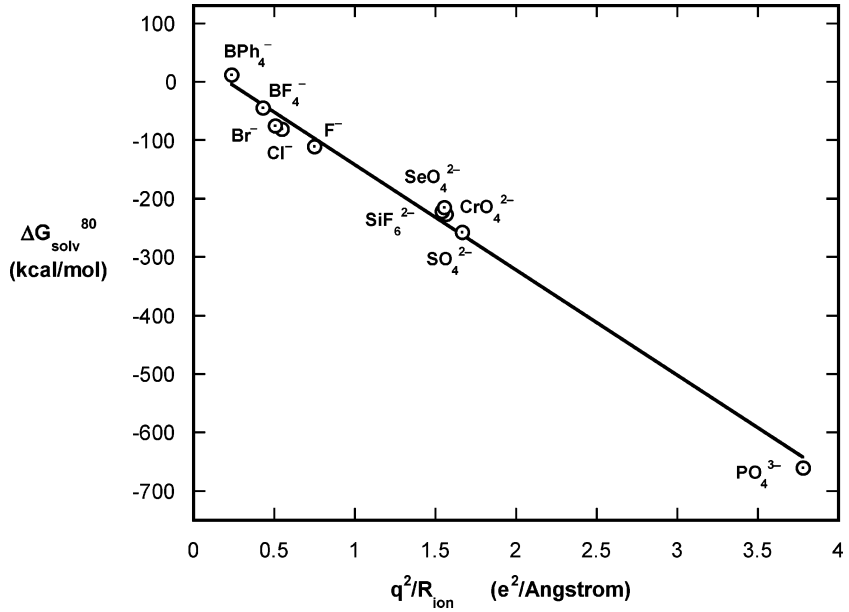

Figure 1. Correlation between experimental hydration free energy (ΔG_{solv}^{80}) and q^2/R_{ion}, where q is the net charge and R_{ion} is the Pauling-type ionic radius[37] of a spherical anion. The ΔG_{solv} (in kcal/mol) for PO_4^{3-}, SO_4^{2-}, CrO_4^{2-}, SiF_6^{2-}, SeO_4^{2-}, F^-, Cl^-, Br^-, BF_4^-, and BPh_4^-, taken from ref 37, are −660.8, −258.1, −227.0, −222.3, −215.1, −111.1, −81.3, −75.3, −45.4, and 12.0, respectively. The corresponding R_{ion} (in Å) values, also taken from ref 37, are 2.38, 2.40, 2.55, 2.59, 2.57, 1.33, 1.81, 1.96, 2.32, and 4.21.

Table 3. Calculated and Experimental Solvation Free Energies (in kcal/mol) of the Compounds under Study

compound	ΔG_{solv}(calcd)	ΔG_{solv}(expt)
SO_4^{2-}	−257.3	−258.1[a]
MoO_4^{2-}	−230.1	
WO_4^{2-}	−226.9	
CH_3OH	−5.6	−5.1[b]
$HCONH_2$	−9.3	−9.7[b,c]
$CH_3NH_3^+$	−69.6	−70.0[b]

[a] From Marcus.[37] [b] From Chambers et al..[38] [c] Measured for acetamide.

at the S-VWN/6-311++G(2df,2p) level yielded solvation free energies of the studied species that are close to the experimental data (Table 3).

XO_4·(Formamide)$_n$ Structures. A. Dependence on *n*. Figure 2 shows the interaction between a formamide and the oxyanion and how this interaction changes with increasing number of formamide ligands, *n*, in the complex. Formamide interacts with the oxyanion via one of the amino protons forming a strong N−H···O hydrogen bond (Figure 2). Another weaker hydrogen bond between the carbonyl proton and an anionic oxygen also helps to stabilize the complex. As *n* increases, the N−H···O distance increases, while the respective X−O (X = S, Mo, W) bond length decreases (Figure 2). This, on one hand, is due to the increased steric repulsion among the ligands when *n* increases and, on the other, to the decreased incremental charge transfer from the oxyanion to the ligand in the bulkier complexes, leading to weaker interactions with the individual ligands. The incremental net charge transfer from SO_4^{2-} to $HCONH_2$ is −0.23e but decreases to −0.07e, −0.04e, and −0.03e with each additional formamide.

B. Dependence on X. The interaction between the oxyanion and formamide is also affected by the nature of the oxyanion. Among the three dianions, SO_4^{2-} has the highest bond-order value,[20] enabling it to donate more electron density to the ligand. Consequently, it yields the shortest N−H···O hydrogen bond (1.28 Å) in the single-ligand complexes, as compared to Mo (1.32 Å) and W (1.37 Å) (see Figure 2A). These bond distances anticorrelate with the amount of the net charge transferred from each of the three oxyanions to the ligand, which decreases from −0.23e in the sulfate−monoformamide complex to −0.21e and −0.19e in the respective molybdate and tungstate complexes. With further size increase of the complex upon adding more formamide ligands, the effect of the charge transfer on the cluster's geometry diminishes: the incremental charge-transfer values for the largest, tetracoordinate complexes are similar (∼ −0.03e) and, correspondingly, the ligand−oxyanion bond distances in the series converge (∼1.60−1.61 Å, Figure 2D).

XO_4·(Methanol)$_n$ Structures. A. Similarities with XO_4·(Formamide)$_n$ Structures. Figure 3 shows the interaction between a methanol and the oxyanion and how this interaction changes with increasing number of methanol ligands, *n*, in the complex. Methanol binds the oxyanion via its hydroxyl proton (forming a strong O−H···O hydrogen bond) and one of the methyl protons (forming a weaker hydrogen bond with another anionic oxygen, see Figure 3). As found for the [XO_4·(formamide)$_n$] (X = S, Mo, W) complexes, the ligand−oxyanion distances increase, while the X−O bond lengths decrease with increasing *n* (Figure 3). Furthermore, in both types of tetracoordinate $[XO_4{\cdot}L_4]^{2-}$ (L = $HCONH_2$, MeOH) complexes, the H−O(S) distances (1.61 and 1.55 Å) are slightly longer than the respective H−O(Mo/W) distances (1.60 and 1.54 Å), probably because of the greater steric repulsion among the ligands in the vicinity of the smaller sulfate anion.

B. Differences between XO_4·(Methanol)$_n$ and XO_4·(Formamide)$_n$ Structures. Comparison of the ligand−oxyanion distances in Figures 2A and 3A shows that the H···O bond distances in the single-methanol complexes are much longer than those in the respective single-amide complexes. This can be attributed to two factors: (1) Methanol has a lower polarizability (calculated mean static polarizability $\bar{\alpha}$ = 20.9 Å^3) than formamide ($\bar{\alpha}$ = 27.8 Å^3). (2) It is a poorer charge acceptor than formamide, as evidenced by a charge transfer from

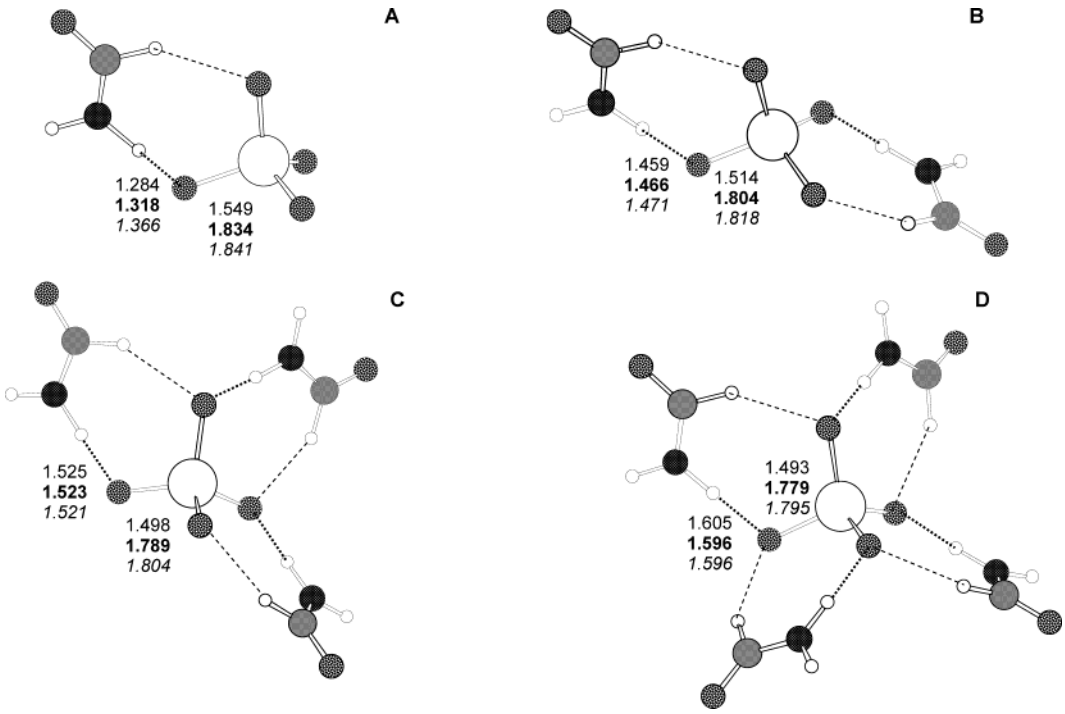

Figure 2. Fully optimized S-VWN/6-311++G(2df,2p) structures of XO_4^{2-} (X = S, Mo, W) complexed with formamide(s). Bond lengths (in Å) are given in normal, **bold**, and *italic* fonts for SO_4^{2-}, $\mathbf{MoO_4^{2-}}$, and WO_4^{2-} complexes, respectively. The dotted and dashed lines denote respectively strong hydrogen bonds (NH···O < 2.0 Å and N−Ĥ...O = 180 ± 30°) and weak hydrogen bonds (2.0 ≤ CH···O < 2.4 Å and C−Ĥ...O = 180 ± 60°).

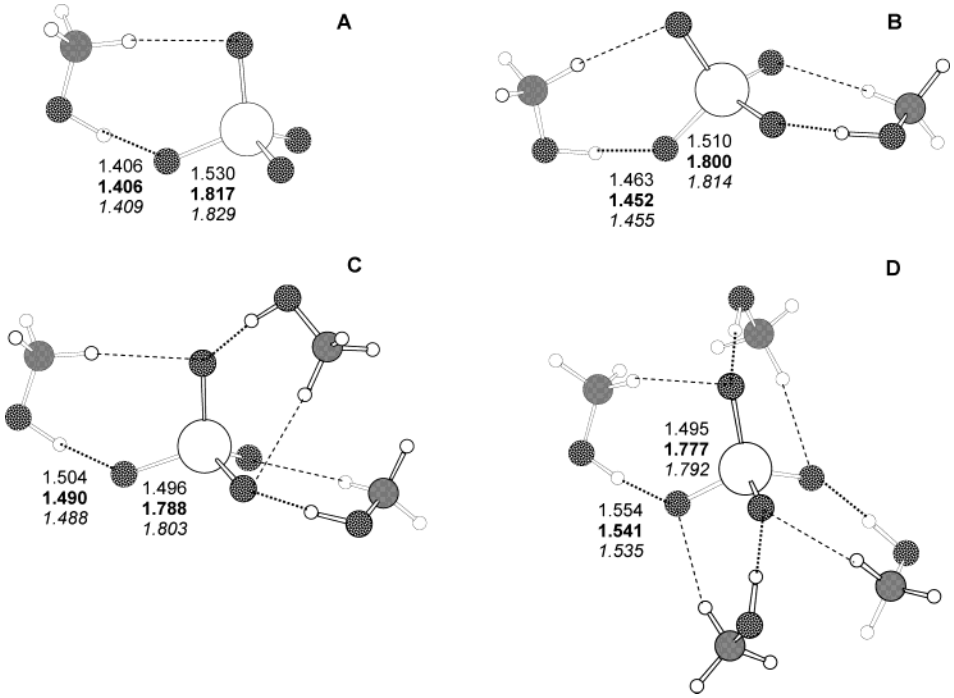

Figure 3. Fully optimized S-VWN/6-311++G(2df,2p) structures of XO_4^{2-} (X = S, Mo, W) complexed with methanol(s). Bond lengths (in Å) are given in normal, **bold**, and *italic* fonts for SO_4^{2-}, $\mathbf{MoO_4^{2-}}$, and WO_4^{2-} complexes, respectively. The dotted and dashed lines denote respectively strong hydrogen bonds (OH···O < 2.0 Å and O−Ĥ...O = 180 ± 30°) and weak hydrogen bonds (2.0 ≤ CH···O < 2.6 Å and C−Ĥ...O = 180 ± 40°).

SO_4^{2-} to methanol and formamide of −0.17e and −0.23e, respectively. However, relative to $[SO_4{\cdot}HCONH_2]^{2-}$, the smaller charge reduction on SO_4^{2-} in $[SO_4{\cdot}CH_3OH]^{2-}$ allows the oxyanion to donate more charge to the next methanol; hence, the charge transfer to the second (−0.11e), third (−0.06e), and fourth (−0.04e) methanol ligands are larger than that to the second (−0.07e), third (−0.04e), and fourth (−0.03e) formamide ligands. This eventually results in shorter ligand−oxyanion bond distances in complexes containing three and four methanol ligands, as compared to the respective formamide complexes (compare Figure 2C, D with Figure 3C, D).

Another difference between the formamide and methanol complexes lies in the trends of H···O(X) hydrogen bond distances as a function of X, where X = S, Mo, and W. In contrast to the formamide complexes, the single methanol complexes exhibit similar H···O(X) distances (1.41 Å), ir-

Table 4. Energies (ΔE_{elec}), Enthalpies (ΔH^1), and Free Energies (ΔG^x) of $SO_4^{2-} \rightarrow MoO_4^{2-}/WO_4^{2-}$ Exchange in Complexes with Formamide and Methanol Ligands for Media of Different Dielectric Constant x[a]

	reactant[b]	product[b] + SO_4^{2-}	ΔE_{elec}	ΔH^1	ΔG^1	ΔG^4	ΔG^{10}	ΔG^{20}	ΔG^{80}
	+ MoO_4^{2-}								
1	$[SO_4 \cdot form]^{2-}$	$[MoO_4 \cdot form]^{2-}$	2.4	2.5	2.6	−7.8	−9.4	−9.8	−10.2
2	$[SO_4 \cdot (form)_2]^{2-}$	$[MoO_4 \cdot (form)_2]^{2-}$	4.1	4.0	4.6	−9.0	−11.1	−11.6	−12.4
3	$[SO_4 \cdot (form)_3]^{2-}$	$[MoO_4 \cdot (form)_3]^{2-}$	6.0	5.7	7.4	−10.0	−12.8	−13.6	−14.2
4	$[SO_4 \cdot (form)_4]^{2-}$	$[MoO_4 \cdot (form)_4]^{2-}$	7.1	6.7	7.2	−12.3	−15.6	−16.5	−17.2
5[c]	$[SO_4 \cdot (form)_5]^{2-}$	$[MoO_4 \cdot (form)_5]^{2-}$	8.0			−12.4	−15.9	−16.9	−17.7
6[c]	$[SO_4 \cdot (form)_6]^{2-}$	$[MoO_4 \cdot (form)_6]^{2-}$	8.7			−11.5	−15.0	−16.0	−16.9
7[c]	$[SO_4 \cdot (form)_7]^{2-}$	$[MoO_4 \cdot (form)_7]^{2-}$	8.8			−11.6	−15.2	−16.3	−17.2
	+ WO_4^{2-}								
8	$[SO_4 \cdot form]^{2-}$	$[WO_4 \cdot form]^{2-}$	2.6	3.0	3.9	−8.0	−9.9	−10.4	−10.9
9	$[SO_4 \cdot (form)_2]^{2-}$	$[WO_4 \cdot (form)_2]^{2-}$	4.1	4.0	4.6	−11.0	−13.4	−14.1	−14.7
10	$[SO_4 \cdot (form)_3]^{2-}$	$[WO_4 \cdot (form)_3]^{2-}$	5.9	5.6	7.1	−12.8	−15.8	−16.6	−17.4
11	$[SO_4 \cdot (form)_4]^{2-}$	$[WO_4 \cdot (form)_4]^{2-}$	6.9	6.4	6.5	−15.2	−18.7	−19.6	−20.4
	+ MoO_4^{2-}								
12	$[SO_4 \cdot MeOH]^{2-}$	$[MoO_4 \cdot MeOH]^{2-}$	1.1	1.2	1.0	−9.1	−10.5	−10.9	−11.2
13	$[SO_4 \cdot (MeOH)_2]^{2-}$	$[MoO_4 \cdot (MeOH)_2]^{2-}$	2.1	2.0	2.9	−9.2	−10.8	−11.3	−11.8
14	$[SO_4 \cdot (MeOH)_3]^{2-}$	$[MoO_4 \cdot (MeOH)_3]^{2-}$	4.9	4.6	4.8	−10.1	−12.4	−13.0	−13.6
15	$[SO_4 \cdot (MeOH)_4]^{2-}$	$[MoO_4 \cdot (MeOH)_4]^{2-}$	6.6	6.1	6.9	−9.7	−12.0	−12.5	−13.1
	+ WO_4^{2-}								
16	$[SO_4 \cdot MeOH]^{2-}$	$[WO_4 \cdot MeOH]^{2-}$	0.9	1.0	0.8	−9.6	−11.1	−11.5	−11.9
17	$[SO_4 \cdot (MeOH)_2]^{2-}$	$[WO_4 \cdot (MeOH)_2]^{2-}$	1.4	1.4	2.2	−10.4	−12.1	−12.5	−12.9
18	$[SO_4 \cdot (MeOH)_3]^{2-}$	$[WO_4 \cdot (MeOH)_3]^{2-}$	4.1	3.8	4.0	−12.7	−15.2	−15.9	−16.5
19	$[SO_4 \cdot (MeOH)_4]^{2-}$	$[WO_4 \cdot (MeOH)_4]^{2-}$	5.9	5.4	6.3	−12.5	−15.0	−15.5	−16.1

[a] All energies in kcal/mol; $x = 1$ corresponds to gas-phase values, whereas $x = 4$, 10, 20, and 80 represent increasing solvent exposure of the binding site with $x = 80$, indicating a fully solvent exposed site. [b] form = $HCONH_2$ and MeOH = CH_3OH. [c] ΔG^x are evaluated using eq 4 with $\Delta G^1 \approx \Delta E_{elec}$.

respective of the nature of the oxyanion, but in the largest $[(XO_4) \cdot (CH_3OH)_4]^{2-}$ complexes, H···O(S) > H···O(Mo) > H···O(W) (Figure 3D). The latter bond distances anticorrelate with the amount of incremental charge transferred from XO_4^{2-} to the four methanol ligands, which is 0.043e for sulfate, 0.044e for molybdate, and 0.047e for tungstate complexes.

Free Energies of $SO_4^{2-} \rightarrow MoO_4^{2-}/WO_4^{2-}$ Exchange in Dianionic Complexes. The free energies (ΔG^x) for replacing SO_4^{2-} with MoO_4^{2-}/WO_4^{2-} in complexes with formamide and methanol ligands in Table 4 show that the anion−ligand interaction effects are opposite to solvation effects. All the electronic energies/enthalpies in Table 4 are positive and become more positive with increasing number of ligands in the complex. The gas-phase free energies, which are dictated by the corresponding electronic energies/enthalpies, are also all positive implying that the exchange reactions in the gas phase are unlikely. This is partly because relative to molybdate or tungstate, SO_4^{2-} donates more electron density to the ligands and, thus, has more favorable interactions with formamide and methanol. Solvation, however, reverses the gas-phase trend; all the condensed-phase free energies ΔG^x ($x \geq 4$) are negative and become more negative with increasing solvent accessibility of the complex, implying that molybdate and tungstate can displace sulfate from sulfate-formamide/methanol complexes in buried or solvent-exposed sites. Furthermore, increasing the number of formamide ligands, n, in the $[(SO_4) \cdot (form)_n]^{2-}$ complex from 1 to 4 favors the $SO_4^{2-} \rightarrow MoO_4^{2-}/WO_4^{2-}$ exchange in the condensed phase; however, a further increase of n from 5 to 7 resulted in roughly constant ΔG^x ($x \geq 4$) for $SO_4^{2-} \rightarrow MoO_4^{2-}$ exchange. In methanol complexes, this "saturation" appears to occur earlier starting from the tricoordinated complex (Table 4, reactions 14−15 and 18−19).

Why does solvation have such a dramatic effect on the thermodynamics of replacing SO_4^{2-} in $[(SO_4) \cdot L_n]^{2-}$ complexes with MoO_4^{2-}/WO_4^{2-} (eq 1)? Analysis of the individual components in eq 4 (see Scheme 1) reveals that the thermodynamics of eq 1 is dictated by the large ΔG_{solv} difference between the *isolated* dianions, SO_4^{2-} and MoO_4^{2-}/WO_4^{2-}, which in turn reflects their size difference (see Table 1 and Figure 1). The $\Delta\Delta G_{solv}$ differences for $\epsilon = 4$ are the following:

$$\Delta G_{solv}{}^4(SO_4) - \Delta G_{solv}{}^4(MoO_4) = -191.7 - (-170.5) = -21.2 \text{ kcal/mol} \quad (6a)$$

$$\Delta G_{solv}{}^4(SO_4) - \Delta G_{solv}{}^4(WO_4) = -191.7 - (-167.6) = -24.1 \text{ kcal/mol} \quad (6b)$$

while the $\Delta\Delta G_{solv}$ differences for $\epsilon = 80$ are

$$\Delta G_{solv}{}^{80}(SO_4) - \Delta G_{solv}{}^{80}(MoO_4) = -257.3 - (-230.1) = -27.2 \text{ kcal/mol} \quad (6c)$$

$$\Delta G_{solv}{}^{80}(SO_4) - \Delta G_{solv}{}^{80}(WO_4) = -257.3 - (-226.9) = -30.4 \text{ kcal/mol} \quad (6d)$$

With the successive complexation of ligands to the oxyanion, the size difference between sulfate and molybdate/tungstate *complexes* decreases and, hence, the solvation free energy difference between the respective clusters narrows. For example, in the case of the tetraformamide complexes $[(XO_4) \cdot (HCONH_2)_4]^{2-}$, the distances from X = S, Mo, and W to the farthest atom are 5.26, 5.33, and 5.35 Å, respectively. The slight size difference between sulfate and molybdate/tungstate *complexes* correlates with the dramatically smaller $\Delta\Delta G_{solv}$ differences for both buried and solvent-exposed $[(XO_4) \cdot (HCONH_2)_4]^{2-}$ oxy-

Table 5. Enthalpies (ΔH^1) and Free Energies (ΔG^x) of $[(SO_4)\cdot(L)_2\cdot(CH_3NH_3)_2]^0 + XO_4^{2-} \rightarrow [(XO_4)\cdot(L)_2\cdot(CH_3NH_3)_2]^0 + SO_4^{2-}$, Where X = Mo/W for Media of Different Dielectric Constant x[a]

L	X	ΔH^1	ΔG^1	ΔG^4	ΔG^{10}	ΔG^{20}	ΔG^{80}
$HCONH_2$	Mo	11.7	11.9	−9.0	−12.8	−13.9	−14.8
$HCONH_2$	W	13.2	13.8	−10.2	−14.5	−15.7	−16.8
CH_3OH	Mo	11.8	13.3	−6.7	−10.2	−11.1	−11.9
CH_3OH	W	12.7	14.0	−8.9	−12.8	−13.8	−14.7

[a] See footnote to Table 4.

anion complexes, as compared to the *isolated* oxyanions (eq 6):

$$\Delta G_{solv}{}^4[(SO_4)\cdot(HCONH_2)_4]^{2-} - \Delta G_{solv}{}^4[(MoO_4)\cdot(HCONH_2)_4]^{2-} = -1.7 \text{ kcal/mol} \quad (7a)$$

$$\Delta G_{solv}{}^4[(SO_4)\cdot(HCONH_2)_4]^{2-} - \Delta G_{solv}{}^4[(WO_4)\cdot(HCONH_2)_4]^{2-} = -2.4 \text{ kcal/mol} \quad (7b)$$

while

$$\Delta G_{solv}{}^{80}[(SO_4)\cdot(HCONH_2)_4]^{2-} - \Delta G_{solv}{}^{80}[(MoO_4)\cdot(HCONH_2)_4]^{2-} = -2.8 \text{ kcal/mol} \quad (7c)$$

$$\Delta G_{solv}{}^{80}[(SO_4)\cdot(HCONH_2)_4]^{2-} - \Delta G_{solv}{}^{80}[(WO_4)\cdot(HCONH_2)_4]^{2-} = -3.5 \text{ kcal/mol} \quad (7d)$$

Hence, displacing sulfate from $[(SO_4)\cdot L_n]^{2-}$ complexes with molybdate/tungstate in a condensed medium is driven by the greater solvation free energy gain upon releasing SO_4^{2-} relative to the desolvation penalty of MoO_4^{2-}/WO_4^{2-}.

Free Energies of $SO_4^{2-} \rightarrow MoO_4^{2-}/WO_4^{2-}$ Exchange in Neutral Complexes. As SBP and ModA binding sites do not contain any positively charged residues such as Lys or Arg, which are found to electrostatically stabilize the bound dianion in other (nontransport) sulfate and molybdate proteins,[21,22] it is of interest to establish to what extent Lys/Arg might contribute to the binding site affinity/selectivity. Hence, tetracoordinate oxyanion complexes were modeled containing two methylammonium cations (mimicking Lys side chains) and two formamide or methanol ligands, and the free energies ΔG^x of replacing SO_4^{2-} in these complexes with MoO_4^{2-}/WO_4^{2-} were computed (Table 5). In the gas phase, replacing two neutral formamide/methanol ligands in the $[(SO_4)\cdot(HCONH_2)_4]^{2-}/[(SO_4)\cdot(CH_3OH)_4]^{2-}$ complexes with two positively charged $CH_3NH_3^+$ ligands disfavors $SO_4^{2-} \rightarrow MoO_4^{2-}/WO_4^{2-}$ exchange, as the ΔG^1 in Table 5 are more positive than the respective ΔG^1 in Table 4 (reactions 4, 11, 15, and 19). This is probably because of the greater loss of favorable charge−charge interactions, as compared to charge-dipole interactions upon $SO_4^{2-} \rightarrow MoO_4^{2-}/WO_4^{2-}$ exchange. In condensed media, replacing two formamide/methanol ligands in the tetraformamide/methanol complex with two $CH_3NH_3^+$ makes the $SO_4^{2-} \rightarrow MoO_4^{2-}/WO_4^{2-}$ exchange less favorable, as the ΔG^x ($x \geq 4$) values in Table 5 for X = Mo and W, which are similar, are *less negative* than their counterparts in Table 4 (reactions 4, 11, 15, and 19). However, the neutral→cationic ligand substitution in tetraformamide/methanol complex does not change the sign of ΔG^x, indicating that the substitution does not seem to affect binding-site selectivity.

Although introducing positively charged ligands in the complex does not contribute to the selectivity of the oxyanion-binding sites, it does contribute substantially to the stabilization of the anion-binding site: the methanol → methylammonium substitution reaction,

$$[(SO_4)\cdot(CH_3OH)_4]^{2-} + 2CH_3NH_3^+ \leftrightarrow [(SO_4)\cdot(CH_3OH)_2\cdot(CH_3NH_3)_2]^0 + 2CH_3OH \quad (8)$$

is favorable in buried or more solvent exposed binding sites, as evidenced by ΔG^4, ΔG^{10}, and ΔG^{20} of −64.0, −19.9, and −4.9 kcal/mol, respectively.

XO_4^{2-} Interaction Energies in Expanding/Shrinking Cavities. ModA has a larger anion-binding cavity (with an estimated volume of 72−80 Å^3) than SBP (estimated volume of 59−64 Å^3).[16,23] In line with these observations, calculations were performed to assess the role of the binding cavity size in dianion selectivity. As such, we modeled formamide−sulfate interactions in an optimal sulfate cavity and in a larger cavity, the latter mimicking sulfate binding to the ModA anion-binding site. We also modeled formamide−molybdate interactions in an optimal molybdate cavity and in a smaller cavity, the latter mimicking molybdate binding to SBP. All four formamide−sulfate H···O(S) distances in $[(SO_4)\cdot(HCONH_2)_4]^{2-}$ were elongated simultaneously in increments of 0.1 Å starting from the equilibrium distance of 1.605 Å (Figure 2D), while the other internal coordinates were frozen at their equilibrium values. Using the interaction energy at the equilibrium structure as a reference, the relative changes in formamide−sulfate interaction energies ($\Delta\Delta E$) were evaluated for each expanding structure and plotted as a function of the H···O(S) distance (Figure 4A). In analogy, all four formamide−molybdate H···O(Mo) distances in $[(MoO_4)\cdot(HCONH_2)_4]^{2-}$ were shrunk simultaneously in increments of 0.1 Å starting from the equilibrium distance of 1.596 Å (Figure 2D), while the internal coordinates were frozen at their equilibrium values. The resulting $\Delta\Delta E$ values for each shrinking structure are plotted as a function of the H···O(Mo) distance in Figure 4B.

Figure 4A and B show different rates of change of $\Delta\Delta E$ with respect to the oxyanion−formamide distance. Although distorting the molecular geometry from its equilibrium configuration leads, in both cases, to less favorable interaction energies, placing an oxyanion in an expanding cavity leads to less drastic changes in $\Delta\Delta E$ (Figure 4A) than the opposite case of inserting it in a shrinking cavity (Figure 4B). In other words, a large cavity (such as the molybdate-binding site of a molybdenum transport protein) does not strongly resist binding of smaller anions (such as SO_4^{2-}), as evidenced by the gradual increase in binding energy with increasing SO_4^{2-}−ligand distance. In sharp contrast, a small cavity (such as the sulfate-binding site of an SBP) strongly opposes binding of larger anions (such as molybdate and tungstate), as manifested by the steep increase in binding energy with decreasing MoO_4^{2-}−ligand distance. These findings suggest that molybdate-binding sites do not appear to be very anion-size specific, whereas sulfate-binding sites are much more anion-size selective.

Discussion

Assessment of Errors. In computing the oxyanion-exchange free energies in Table 4, systematic errors in the computed gas-

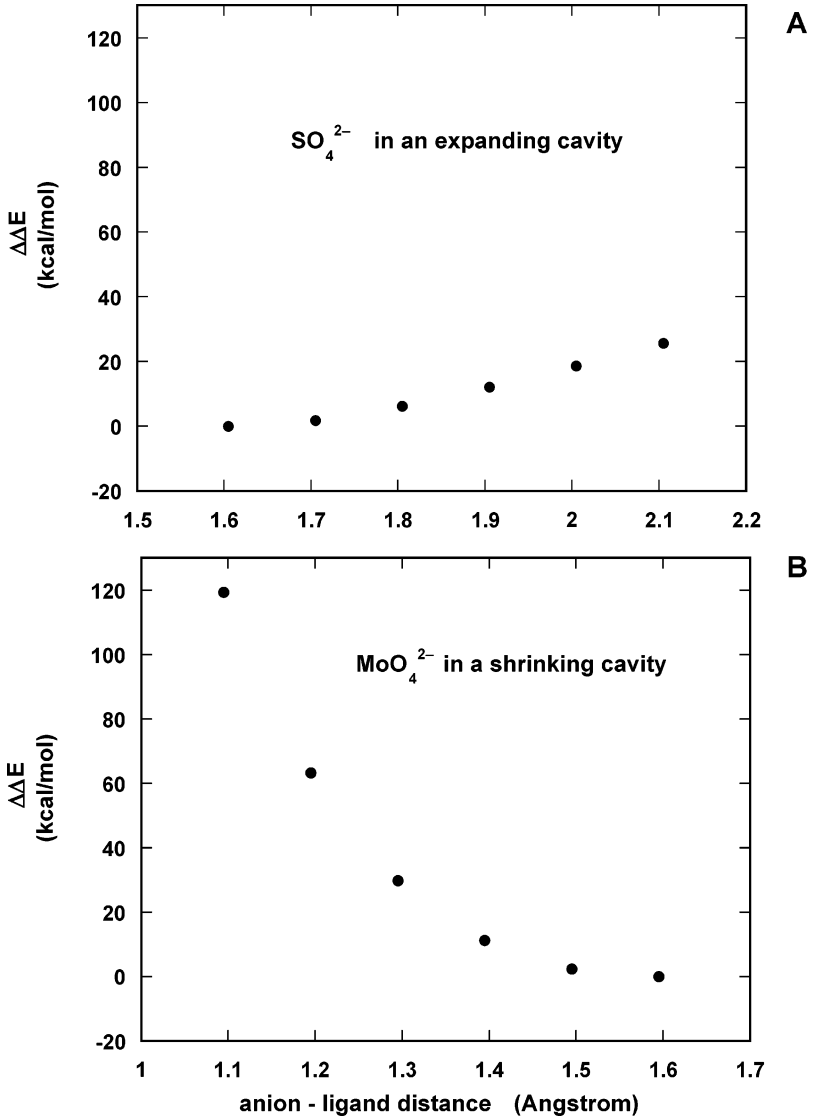

Figure 4. Relative interaction energies, $\Delta\Delta E$ in (A) $[(SO_4)\cdot(HCONH_2)_4]^{2-}$ as a function of (N)H···O(S) bond elongation and (B) $[(MoO_4)\cdot(HCONH_2)_4]^{2-}$ as a function of (N)H···O(Mo) bond shrinkage. The reference energy is the interaction energy at the equilibrium geometry.

phase and solvation free energies of the reactants are likely to partially cancel those of the respective products. Errors in the computed geometries and gas-phase free energies have been minimized by calibrating the methods and basis sets employed (Tables 1 and 2). The $SO_4^{2-} \rightarrow MoO_4^{2-}/WO_4^{2-}$ exchange reaction (eq 1) in the gas phase is enthalpy-driven (Table 4); hence, errors in computing the reaction gas-phase entropy are unlikely to change the key findings of this work. By using a set of atomic radii that have been adjusted to reproduce the experimental hydration free energies of the oxyanions and ligands studied (Table 3), the various approximations made in computing ΔG_{solv}[80] have been taken into account implicitly.[39] Furthermore, because the magnitude of the $\Delta G_{solv}{}^x$ of the isolated oxyanions, XO_4^{2-} (X = S, Mo, and W), are of the same order of magnitude and likewise for their complexes, $[(XO_4)\cdot L_n]^{2-}$, systematic errors in the $\Delta G_{solv}{}^x$ of the reactants and products of eq 1 would further cancel. In addition to calibrating the calculations to available pertinent experimental data, we have also taken care to interpret the results (see Results section) based primarily on the *trends* in the free energy changes of the model reactions, as opposed to *their absolute values*.

Consistency with Experiment. The theoretical findings in Table 4 are in accord with the experimental results. The results in Table 4 show that in $[(MoO_4)\cdot L_n]^{2-}$ complexes, the exchange of molybdate for sulfate in buried or solvent-exposed anion-binding sites is thermodynamically unfavorable (positive ΔG^x, $x \geq 4$, for the reverse of reactions 1−7 and 12−15). This is consistent with the experimental finding that the ModA does not bind sulfate.[15] The results in Table 4 also show similar free energies for the respective molybdate and tungstate reactions (compare reactions 1−4 with 8−11, and 12−15 with 16−19). This is in accord with the fact that the ModA binding pocket cannot discriminate between molybdate and tungstate and binds both anions with similar affinity.[15,19,23]

Factors Governing the Anion Selectivity of Sulfate and Molybdate Transport Proteins. The ligand size has been postulated to be the major determinant of selectivity in ModA and SBP.[15,16] Differences in the oxyanion size not only translate into differences in the anion-binding pockets of the cognate

(38) Chambers, C. C.; Hawkins, G. D.; Cramer, C. J.; Truhlar, D. G. *J. Phys. Chem.* **1996**, *100*, 16385−16398.
(39) Dudev, T.; Lim, C. *J. Am. Chem. Soc.* **2000**, *122*, 11146−11153.

protein but also result in differences in protein residue interactions on one hand and differences in solvent interactions on the other. The calculations reveal that solvation effects make significant contributions to anion selectivity. Largely because of solvation effects, anion-binding sites lined with backbone carbonyls or Asn/Gln side chains (modeled by formamides) or Ser/Thr side chains (modeled by methanol) prefer binding to larger anions, such as molybdate and tungstate, as opposed to smaller anions such as sulfate (Table 4). Thus, molybdate-binding sites appear to be well protected against displacement by sulfate: compared with molybdate, the larger cost of desolvating sulfate disfavors the exchange of molybdate for sulfate (Table 4, reverse of reactions 1−7 and 12−15), while the large and rigid cavity in ModA proteins additionally weakens ligand interactions with sulfate (Figure 4A).

Although solvation effects appear to dictate the anion selectivity of molybdate transport proteins, the size of the anion-binding cavity seems to govern the sulfate selectivity of sulfate transport proteins. Sulfate cannot successfully compete with molybdate/tungstate for a given binding site, as evidenced by the negative ΔG^x ($x \geq 4$) for all the reactions in Table 4. Instead, reducing the anion-binding pocket size inhibits binding of molybdate and tungstate (see Figure 4B). Hence, it seems that the specific protein architecture that restricts the cavity size in sulfate-binding proteins suffices to efficiently select sulfate over molybdate/tungstate.

Why Positively Charged Residues are Absent in SBP and ModA-Binding Sites. The calculations herein also help to explain the absence of positively charged Lys/Arg side chains in the anion-binding sites of SBP and ModA. During evolution, these proteins may have excluded cationic ligands from their binding sites for the following two reasons. First, Lys/Arg do not seem to contribute to the selectivity of the anion-binding pocket (Table 5). Second, they additionally substantially stabilize the complex between the oxyanion and protein ligands. The strong charge−charge interactions between positively charged Arg/Lys residues and the negatively charged oxyanion would, however, prohibit rapid anion dissociation. This may not be advantageous for transport proteins, which have to release the bound substrate at a certain stage during the transport process.

In summary, the results obtained here have shown that different factors dictate the anion selectivity of sulfate and molybdate transport proteins. These findings could help in engineering proteins or in designing synthetic hosts that can selectively recognize inorganic oxyanions such as those studied in this work. In addition to geometric aspects of hydrogen bonding with the guest anion, the size of the anion-binding cavity[16] as well as solvation effects should also be taken into account in developing receptors to bind small and large oxyanions, respectively.

Acknowledgment. We thank Dr. C. Satheesan Babu for helpful discussions. We are grateful to D. Bashford, M. Sommer, and M. Karplus for the program to solve the Poisson equation. This work was supported by the National Science Council, Taiwan (NSC Contract No. 92-2113-M-001-032), and the Institute of Biomedical Sciences, Academia Sinica, Taiwan.

JA047951N